Modelling reveals novel roles of two parallel signalling pathways and homeostatic feedbacks in yeast

Supplementary Information

Jörg Schaber[1*], Rodrigo Baltanas[2&], Alan Bush[2&], Edda Klipp[3*], Alejandro Colman-Lerner[2]

[1] Institute for Experimental Internal Medicine, Medical Faculty, Otto von Guericke University, Magdeburg, Germany

[2] Instituto de Fisiologia, Biologia Molecular y Neurosciencias, Consejo Nacional de Investigaciones Científicas y Técnicas y Facultad de Ciencias Exactas y Naturales, Universidad de Buenos Aires, Buenos Aires, Argentina.

[3] Theoretical Biophysics, Department of Biology, Humboldt University, Berlin, Germany

[&] Equal contribution

[*] To whom correspondence should be addressed:

Jörg Schaber
Email: schaber@med.ovgu.de

Edda Klipp
Email: edda.klipp@rz.hu-berlin.de

Table of Content

1 Model description and selection

The final selected model (Model Nr. 22, Supplementary Tables S8-S10) can be downloaded as a COPASI-file (Version 4.7, Build 34) from the Online Supplementary Material, zipped together with the corresponding data for fitting and prediction (Figure 2, 3A and 3B in the main text). COPASI is freely available from www.COPASI.org. Extract the model and the data files into a common folder and the model fits and predictions can be reproduced by running the parameter estimation task with the method 'Current Solution Statistics'.

Table S1: State variables and their initial conditions. $[\ \ ]_0$ indicate initial concentrations in the osmolytically active volume.

Component	Initial Condition	Remark
V_{os} [fl]	29.5	Osmolytically active volume, derived from a total cell volume of 50 fl and a solid base volume of 41%.
$Pbs2$ [µM]	$Pbs2_t - [Pbs2P]_0 - [Sho1Pbs1]_0$	MAP kinase kinase
$Pbs2P$ [µM]	see Table S2	Activated MAP kinase kinase (Sln1 branch). Initial condition set such that a steady state of Hog1 phosphorylation is maintained.
$Sho1$ [µM]	$Sho1_t - [Sho1Pbs1]_0$	One of the putative upstream sensors
$Sho1Pbs2$ [µM]	see Table S2	Active scaffold complex (Sho1 branch). Initial condition set such that a steady state of Hog1 phosphorylation is maintained.
$Hog1$ [µM]	$Hog1_t - [Hog1P]_0 - [Hog1PP]_0$	MAP kinase
$Hog1P$ [µM]	see Table S2	Single phosphorylated MAP kinase. Initial condition set such that a steady state of Hog1 phosphorylation is maintained.
$Hog1PP$ [µM]	$\frac{Hog1_t \cdot 2.23 \cdot f_n}{100}$	Double phosphorylated, i.e. active, MAP kinase. It was derived from data that 2.23 % of the maximal phosphorylation is the steady state activation. f_n is the fraction in the nucleus at maximal phohsporylation.
RNA [µM]	0.034	Placeholder for transcribed genes. Initial value derived from

		data, i.e. initial percentage of maximum.
$Protein$ [µM]	0.043	Placeholder for Hog1-dependent proteins, especially Gpd1. Initial value derived from measured number of Gpd1 molecules (807, http://yeastgfp.yeastgenome.org)
Gly_{in} [µM]	180000	Intracellular glycerol, approximated by assuming a measured value of 0.1 mM/OD in 1 ml sample (Klipp, et al., 2005) and assuming $18 \cdot 10^6$ cells per ml sample culture and an average osmotic cell volume of 29.5 fl, i.e. $1/18/29.5 \cdot 10^8$.
Gly_{ex} [µM]	1800	Extracellular glycerol, assumed to be 100 times lower than Gly_{in}.
$Fps1$ [µM]	$\frac{Fps1_t}{2}$	Membrane bound open form of aquaglyceroporin Fps1 (assumed to be independent from volume change). Initially half of the channels is assumed to be open.
$Fps1P$ [µM]	$\frac{Fps1_t}{2}$	Membrane bound closed form of aquaglyceroporin Fps1 (assumed to be independent from volume change) . Initially half of the channels is assumed to be closed.
$Phosphatase$ [µM]	0.043	Placeholder for phosphatases like Ppt1/2/3 and others. Initial value derived from measured number of Ptp3 molecules (769, http://yeastgfp.yeastgenome.org)

Table S2: Initial conditions derived from the steady-state assumption. $[\ \ ]_0$ indicate initial concentrations. Bold parameters are free parameters that are estimated from data.

Component	Initial Condition
$Pbs2P$	If both branches are active: $-\left(4\cdot \boldsymbol{k_{Hog1phos1}}\cdot([Hog1PP]_0-Hog1_t)\right)^{-1}\left(\boldsymbol{k_{Hog1dephos}}\cdot[Phosphatase]_0\cdot[Hog1PP]_0+\sqrt{[Hog1PP]_0\cdot(4\cdot Hog1_t-3\cdot[Hog1PP]_0)}\right)$ If only the Sln1 branch is active (k_3=0): $-\left(2\cdot \boldsymbol{k_{Hog1phos1}}^2\cdot([Hog1PP]_0-Hog1_t)\right)^{-1}\left(\boldsymbol{k_{Hog1phos1}}\cdot\boldsymbol{k_{Hog1dephos}}\cdot[Phosphatase]_0\cdot[Hog1PP]_0+\sqrt{\left(\boldsymbol{k_{Hog1phos1}}\cdot\boldsymbol{k_{Hog1dephos}}\cdot[Phosphatase]_0\right)^2\cdot[Hog1PP]_0\cdot(4\cdot Hog1_t-3\cdot[Hog1PP]_0)}\right)$ If only the Sho1 branch is active (k_1=0): 0
$Sho1Pbs$	If both branches are active: $-\left(4\cdot \boldsymbol{k_{Hog1phos2}}\cdot([Hog1PP]_0-Hog1_t)\right)^{-1}\left(\boldsymbol{k_{Hog1dephos}}\cdot[Phosphatase]_0\cdot[Hog1PP]_0+\sqrt{[Hog1PP]_0\cdot(4\cdot Hog1_t-3\cdot[Hog1PP]_0)}\right)$ If only the Sho1 branch is active (k_1=0): $-\left(2\cdot \boldsymbol{k_{Hog1phos2}}^2\cdot([Hog1PP]_0-Hog1_t)\right)^{-1}\left(\boldsymbol{k_{Hog1phos2}}\cdot\boldsymbol{k_{Hog1dephos}}\cdot[Phosphatase]_0\cdot[Hog1PP]_0+\sqrt{\left(\boldsymbol{k_{Hog1phos2}}\cdot\boldsymbol{k_{Hog1dephos}}\cdot[Phosphatase]_0\right)^2\cdot[Hog1PP]_0\cdot(4\cdot Hog1_t-3\cdot[Hog1PP]_0)}\right)$ If only the Sln1 branch is active (k_3=0): 0
$Hog1P$	If both branches are active: $\frac{\mathbf{1}}{\mathbf{2}}\left(-[Hog1PP]_0+\sqrt{[Hog1PP]_0\cdot(4\cdot Hog1_t-3\cdot[Hog1PP]_0)}\right)$ If only the Sln1 branch is active (k_3=0): $\left(2\cdot \boldsymbol{k_{Hog1phos1}}\cdot\boldsymbol{k_{Hog1dephos}}\cdot[Phosphatase]_0\right)^{-1}\left(-\boldsymbol{k_{Hog1phos1}}\cdot\boldsymbol{k_{Hog1dephos}}\cdot[Phosphatase]_0\cdot[Hog1PP]_0+\sqrt{\left(\boldsymbol{k_{Hog1phos1}}\cdot\boldsymbol{k_{Hog1dephos}}\cdot[Phosphatase]_0\right)^2\cdot[Hog1PP]_0\cdot(4\cdot Hog1_t-3\cdot[Hog1PP]_0)}\right)$ If only the Sho1 branch is active (k_1=0): $\left(2\cdot \boldsymbol{k_{Hog1phos2}}\cdot\boldsymbol{k_{Hog1dephos}}\cdot[Phosphatase]_0\right)^{-1}\left(-\boldsymbol{k_{Hog1phos2}}\cdot\boldsymbol{k_{Hog1dephos}}\cdot[Phosphatase]_0\cdot[Hog1PP]_0+\sqrt{\left(\boldsymbol{k_{Hog1phos2}}\cdot\boldsymbol{k_{Hog1dephos}}\cdot[Phosphatase]_0\right)^2\cdot[Hog1PP]_0\cdot(4\cdot Hog1_t-3\cdot[Hog1PP]_0)}\right)$

Table S3: Ordinary differential equation system of the master model. Rates and subscrits in {} indicate optional reactions depending on the candidate model. Volumes are in fl, concentrations in µM and pressure in MPa.

ODEs

$$\frac{dV_{os}}{dt} = -L_p \cdot A \cdot (Turgor + f_{c2p} \cdot R \cdot T \cdot (Osm_{ex} - Osm_{in})$$

$$\frac{d([Pbs2] \cdot V_{os})}{dt} = V_{os} \cdot \left(-\{v_1, v_{1,\mathrm{fb}}\} + v_2 - \{v_3, v_{3,\mathrm{fb}}\} + v_4\right)$$

$$\frac{d([Pbs2P] \cdot V_{os})}{dt} = V_{os} \cdot \left(\{v_1, v_{1,\mathrm{fb}}\} - v_2\right)$$

$$\frac{d([Sho1] \cdot V_{os})}{dt} = V_{os} \cdot \left(-\{v_3, v_{3,\mathrm{fb}}\} + v_4\right)$$

$$\frac{d([Sho1Pbs2\ ] \cdot V_{os})}{dt} = V_{os} \cdot \left(\{v_3, v_{3,\mathrm{fb}}\} - v_4\right)$$

$$\frac{d([Hog1] \cdot V_{os})}{dt} = V_{os} \cdot (-v_5 + v_6)$$

$$\frac{d([Hog1P] \cdot V_{os})}{dt} = V_{os} \cdot (v_5 - v_6 - v_7 + v_8)$$

$$\frac{d([Hog1PP] \cdot V_{os})}{dt} = V_{os} \cdot (v_7 - v_8)$$

$$\frac{d([RNA] \cdot V_{os})}{dt} = V_{os} \cdot (v_9 - v_{10})$$

$$\frac{d([Protein] \cdot V_{os})}{dt} = V_{os} \cdot (v_9 - v_{10})$$

$$\frac{d([Gly_{in}] \cdot V_{os})}{dt} = V_{os} \cdot v_{13} - v_{14}$$

$$\frac{d([Gly_{ex}] \cdot V_{ex})}{dt} = v_{14}$$

$$\frac{d[Fps1]}{dt} = -\{v_{15_1}, v_{15_2}, v_{15_3}, v_{15_4}, v_{15_5}\} + \{v_{16\_1}, v_{16\_2}, v_{16\_3}, v_{16\_4}, v_{16\_5}, v_{16\_6}, v_{16\_7}, v_{16\_8}\}$$

$$\frac{d[Fps1P]}{dt} = \{v_{15_1}, v_{15_2}, v_{15_3}, v_{15_4}, v_{15_5}\} - \{v_{16\_1}, v_{16\_2}, v_{16\_3}, v_{16\_4}, v_{16\_5}, v_{16\_6}, v_{16\_7}, v_{16\_8}\}$$

$$\frac{d([Phosphatase] \cdot V_{os})}{dt} = 0$$

Table S4: Rate equations of the master model. Concentrations are denoted by []. Bold parameters are free parameters that are estimated from data. The other parameters and auxiliary variables are described in Table S5 and S6, respectively. Volumes are in fl, concentrations in μM and pressure in MPa.

Rate	Rate equation	Description and Rationale
v_1	$\boldsymbol{k_1} \cdot Sln1_{Activ} \cdot [Pbs2]$	Simple cell surface area dependent linear activation of Pbs2 through the Sln1 branch.
$v_{1,fb}$	$\frac{\boldsymbol{k_1} \cdot Sln1_{Activ\_fb} \cdot [Pbs2]}{1 + \left(\frac{[Hog1PP]}{\boldsymbol{K_{i,1}}}\right)^{\boldsymbol{h_1}}}$	Simple cell surface area dependent linear activation of Pbs2 through the Sln1 branch, with transient inhibition by activated Hog1.
v_2	$\boldsymbol{k_2} \cdot [Phosphatase] \cdot [Pbs2P]$	Constitutive phosphatase dependent deactivation.
v_3	$\boldsymbol{k_3} \cdot Sho1_{Activ} \cdot [Pbs2] \cdot [Sho1]$	Simple cell surface area dependent binding of Pbs2 to Sho1. The complex is supposed to be the active form.
$v_{3,f}$	$\frac{\boldsymbol{k_3} \cdot Sho1_{Activ\_fb} \cdot [Pbs2] \cdot [Sho1]}{1 + \left(\frac{[Hog1PP]}{\boldsymbol{K_{i,3}}}\right)^{\boldsymbol{h_3}}}$	Simple cell surface area dependent binding of Pbs2 to Sho1. The complex is supposed to be the active form. With transient inhibition by activated Hog1.
v_4	$\boldsymbol{k_4} \cdot [Sho1Pbs2P]$	Constitutive dissociation of the scaffold complex.
v_5	$\boldsymbol{k_{Hog1phos1}} \cdot [Sho1Pbs2] \cdot [Hog1] +$ $\boldsymbol{k_{Hog1phos2}} \cdot [Pbs2P] \cdot [Hog1]$	Linear phosphorylation of Hog1 by either the scaffold complex (Sho1-branch) or activated Pbs2 (Sln1-branch).
v_6	$\boldsymbol{k_{Hog1dephos}} \cdot [Phosphatase] \cdot [Hog1P]$	Constitutive phosphatase dependent de-phosphorylation.
v_7	$\boldsymbol{k_{Hog1phos1}} \cdot [Sho1Pbs2] \cdot [Hog1P] +$ $\boldsymbol{k_{Hog1phos2}} \cdot [Pbs2P] \cdot [Hog1P]$	Linear phosphorylation of Hog1 by either the scaffold complex (Sho1-branch) or activated Pbs2 (Sln1-

		branch).
v_8	$\boldsymbol{k_{Hog1dephos}} \cdot [Phosphatase] \cdot [Hog1PP]$	Constitutive phosphatase dependent de-phosphorylation.
v_9	$\frac{\boldsymbol{k_9} \cdot [Hog1PP]}{\boldsymbol{Km_9} + [Hog1PP]}$	Gene transcription. Hog1 mediated transcription also involves other proteins that are potentially limiting a saturation kinetic is assumed.
v_{10}	$k_{10} \cdot [RNA]$	$mRNA$ degradation
v_{11}	$\boldsymbol{k_{11}} \cdot [RNA]$	Protein/enzyme production
v_{12}	$k_{12} \cdot [Protein]$	Protein/enzyme degradation
v_{13}	$\frac{\boldsymbol{k_{13\_1}} \cdot [Protein] \cdot (1 + \boldsymbol{k_{13\_2}} \cdot [Hog1PP])}{\boldsymbol{Km_{13}} + [Protein] \cdot (1 + \boldsymbol{k_{13\_2}} \cdot [Hog1PP])}$	Glycerol production. As glycerol concentration also involves other proteins and cofactors that are potentially limiting a saturation kinetic is assumed. In addition, effective enzyme concentration can be enhanced as a function of activated Hog1.
v_{14}	$k_{tr} \cdot k_s \cdot ([Gly_{in}] - [Gly_{ex}])$	Gradient driven glycerol flow out of the cell, where k_{tr} characterises the state of the aquaglyceroporin channel Fps1 and k_s the maximal transport capacity of the channel.
$v_{15\_\{1,2,3,4\}}$	$\boldsymbol{k_{15}} \cdot Fps1_{Activ\_\{1,2,3,4\}} \cdot [Fps1]$	Volume dependent closure of Fps1, in conjunction with v_{16_1}, v_{16_2}, v_{16_3} and v_{16_4}, respectively.
v_{15_5}	$\boldsymbol{k_{15}} \cdot Turgor_{Deactiv} \cdot [Fps1]$	Turgor dependent closure of Fps1, in conjunction with v_{16_5}, v_{16_6}, v_{16_7}, v_{16_8}.
v_{16_1}	$\boldsymbol{k_{16}} \cdot [Fps1P]$	Constitutive channel opening v_{16_5}, in conjunction with v_{15_1}.

v_{16_2}	$\frac{\boldsymbol{k_{16}} \cdot [Fps1P]}{1 + \left(\frac{[Hog1PP]}{\boldsymbol{K_{i,16}}}\right)^{\boldsymbol{h_{16}}}}$	Activated Hog1 inhibited channel opening, in conjunction with v_{15_2}.
v_{16_3}	$\boldsymbol{k_{16}} \cdot Turgor_{Activ} \cdot [Fps1P]$	Turgor dependent channel opening, in conjunction with v_{15_3}.
v_{16_4}	$\frac{\boldsymbol{k_{16}} \cdot Turgor_{Activ} \cdot [Fps1P]}{1 + \left(\frac{[Hog1PP]}{\boldsymbol{K_{i,16}}}\right)^{\boldsymbol{h_{16}}}}$	Turgor dependent channel opening, inhibited by activated Hog1, in conjunction with v_{15_4}.
v_{16_5}	$k_{16\_5} \cdot [Fps1P]$	Constitutive channel opening, in conjunction with v_{15_5}.
v_{16_6}	$\frac{k_{16\_6} \cdot [Fps1P]}{1 + \left(\frac{[Hog1PP]}{\boldsymbol{K_{i,16}}}\right)^{\boldsymbol{h_{16}}}}$	Activated Hog1 inhibited channel opening, in conjunction with v_{15_5}.
v_{16_7}	$k_{16\_7} \cdot Turgor_{Activ} \cdot [Fps1P]$	Turgor dependent channel opening, in conjunction with v_{15_5}.
v_{16_8}	$\frac{k_{16\_8} \cdot Turgor_{Activ} \cdot [Fps1P]}{1 + \left(\frac{[Hog1PP]}{\boldsymbol{K_{i,16}}}\right)^{\boldsymbol{h_{16}}}}$	Turgor dependent channel opening inhibited by activated Hog1, in conjunction with v_{15_5}.
v_{17_1}	k_{17_1}	Fps1 production, in conjunction with v_{18}.
v_{17_2}	k_{17_2}	Fps1 production, in conjunction with v_{18_1}.
v_{18_1}	$\boldsymbol{k_{18}} \cdot [Hog1PP] \cdot [Fps1]$	Hog1 dependent Fps1 degradation/internalisation, in conjunction with v_{17_1}.
v_{18_2}	$\boldsymbol{k_{18}} \cdot [Protein] \cdot [Fps1]$	Protein dependent Fps1 degradation/ internalisation, in conjunction with v_{17_2}.

Table S5: Auxiliary parameters and variables. Concentrations are denoted by []. Bold parameters are free parameters that are estimated from data. Volumes are in fl, concentrations in μM and pressures in MPa.

Variable	Definition	Description
V_b	$V_0 f_{min}$	Solid or minimal volume of the cell.
V	$V_{os} + V_b$	Total cell volume.
V_{os_0}	$V_0(1 - f_{min})$	Initial osmotically active volume.
$V_{P=0}$	$V_0 e^{\frac{P_0}{\varepsilon}}$	Non-turgid volume.
A	$(36\pi)^{1/3} V^{2/3}$	Total cell surface area.
$f_{n2\mu M}$	$10^{21} mol^{-1} {V_{os}}_0^{-1}$	Factor converting number of molecules in μM concentrations per cell.
c_0^i	$c_0^e + \frac{P_0}{f_{c2p} RT}$	Initial total cellular osmolyte concentration.
c_0^{in}	$c_0^i - [Gly_{in}]$	Initial non-permeable cellular osmolyte concentration.
c_n^e	$c_0^e - [Gly_{ex}] + \left(1 - e^{\frac{t_s - t}{t_m}}\right) 2\theta c_{NaCl} 10^6$	Osmotic salt shock. Starts at time t_s and has a certain mixing time t_m.

Osm_{in}	$[Gly_{in}] + \frac{c_0^{in} V_{os_0}}{V_{os}}$	Intracellular osmolytically active concentration.
Osm_{ex}	$c_n^e + [Gly_{ex}]$	Extracellular osmolytically active concentration.
$Turgor$	$\begin{cases} \varepsilon ln\left(\frac{V}{V_{P=0}}\right) & for\ V > V_{P=0} \\ 0 & else \end{cases}$	Turgor pressure [MPa].
$Sln1_{Activ}$	$\begin{cases} \frac{A_0 - A}{A_0} - Sln1_{offset} & for\ \frac{A_0 - A}{A_0} > Sln1_{offset} \\ 0 & else \end{cases}$	Linear activation function for the Sln1 branch.
$Sln1_{offset}$	$\frac{\boldsymbol{k_2} \cdot [Phosphatase]_0 \cdot [Pbs2P]_0}{\boldsymbol{k_1} \cdot [Pbs2]_0}$	Steady state activation of the Sln1 branch.
$Sln1_{Activ\_fb}$	$\begin{cases} \frac{A_0 - A}{A_0} - Sln1_{offset\_fb} & for\ \frac{A_0 - A}{A_0} > Sln1_{offset} \\ 0 & else \end{cases}$	Linear activation function for the Sln1 branch with feedback.
$Sln1_{offset\_fb}$	$\frac{\boldsymbol{k_2} \cdot [Phosphatase]_0 \cdot [Pbs2P]_0 \cdot \left(1 + \left(\frac{[Hog1PP]_0}{\boldsymbol{K_{i,1}}}\right)^{\boldsymbol{h_1}}\right)}{\boldsymbol{k_1} \cdot [Pbs2]_0}$	Steady state activation of the Sln1 branch with feedback.
$Sho1_{Activ}$	$\begin{cases} \frac{A_0 - A}{A_0} - Sho1_{offset} & for\ \frac{A_0 - A}{A_0} > Sho1_{offset} \\ 0 & else \end{cases}$	Linear activation function for the Sln1 branch.
$Sho1_{offset}$	$\frac{\boldsymbol{k_4} \cdot [Sho1Pbs2P]_0}{\boldsymbol{k_3} \cdot [Pbs2]_0 \cdot [Sho1]_0}$	Steady state activation of the Sln1 branch.

$Sho1_{Activ\_fb}$	$\begin{cases} \frac{A_0 - A}{A_0} - Sho1_{offset\_fb} & for\ \frac{A_0 - A}{A_0} > Sho1_{offset} \\ 0 & else \end{cases}$	Linear activation function for the Sln1 branch with feedback.
$Sho1_{offset\_fb}$	$\frac{\boldsymbol{k_4} \cdot [Sho1Pbs2P]_0 \cdot \left(1 + \left(\frac{[Hog1PP]_0}{\boldsymbol{K_{i,3}}}\right)^{\boldsymbol{h_3}}\right)}{\boldsymbol{k_3} \cdot [Pbs2]_0 \cdot [Sho1]_0}$	Steady state activation of the Sln1 branch with feedback.
k_{10}	$\frac{\frac{\boldsymbol{k_9} \cdot [Hog1PP]_0}{\boldsymbol{Km_9} + [Hog1PP]_0}}{[RNA]_0}$	RNA degradation rate.
k_{12}	$\frac{\boldsymbol{k_{11}} \cdot [RNA]_0}{[Protein]_0}$	Protein degradation rate.
k_{tr}	$\frac{[Fps1]}{Fps1_t}$	Fps1 channel closure.
k_s	$\frac{V_{os_0} \frac{\boldsymbol{k_{13\_1}} \cdot [Protein]_0 \cdot (1 + \boldsymbol{k_{13\_2}} \cdot [Hog1PP]_0)}{\boldsymbol{Km_{13}} + [Protein]_0 \cdot (1 + \boldsymbol{k_{13\_2}} \cdot [Hog1PP]_0)}}{k_{tr_0} \cdot ([Gly_{in}]_0 - [Gly_{ex}]_0)}$	Maximal Fps1 glycerol transport capacity.
$Fps1_{Activ\_\{1-4\}}$	$\begin{cases} \frac{A_0 - A}{A_0} - Fps1_{offset\_\{1-4\}} & for\ \frac{A_0 - A}{A_0} > Fps1_{offset\_\{1-} \\ 0 & else \end{cases}$	Linear activation function for Fps1 closure.
$Fps1_{offset\_1}$	$\frac{\boldsymbol{k_{16}} \cdot [Fps1P]_0}{\boldsymbol{k_{15}} \cdot [Fps1]_0}$	Steady state activation for Fps1 closure.
$Fps1_{offset\_2}$	$\frac{\boldsymbol{k_{16}} \cdot [Fps1P]_0}{\left(1 + \left(\frac{[Hog1PP]_0}{\boldsymbol{K_{i,16}}}\right)^{\boldsymbol{h_{16}}}\right) \boldsymbol{k_{15}} \cdot [Fps1]_0}$	Steady state activation for Fps1 closure.
$Fps1_{offset\_3}$	$\frac{\boldsymbol{k_{16}} \cdot [Fps1P]_0 Turgor_{Activ_0}}{\boldsymbol{k_{15}} \cdot [Fps1]_0}$	Steady state activation for Fps1 closure.
$Fps1_{offset\_4}$	$\frac{\boldsymbol{k_{16}} \cdot [Fps1P]_0 Turgor_{Activ_0}}{\left(1 + \left(\frac{[Hog1PP]_0}{\boldsymbol{K_{i,16}}}\right)^{\boldsymbol{h_{16}}}\right) \boldsymbol{k_{15}} \cdot [Fps1]_0}$	Steady state activation for Fps1 closure.

$Turgor_{Deactiv}$	$1 - \frac{Turgor^{h_{TurgorActiv}}}{P_0^{h_{TurgorActiv}} + Turgor^{h_{TurgorActiv}}}$	Turgor dependent Fps1 closure.
$Turgor_{Activ}$	$\frac{Turgor^{h_{TurgorActiv}}}{P_0^{h_{TurgorActiv}} + Turgor^{h_{TurgorActiv}}}$	Turgor dependent Fps1 opening.
k_{16_5}	$\frac{\boldsymbol{k_{15}} \cdot 0.5 \cdot [Fps1]_0}{[Fps1P]_0}$	
k_{16_6}	$\frac{\boldsymbol{k_{15}} \cdot 0.5 \cdot [Fps1]_0 \left(1 + \left(\frac{[Hog1PP]_0}{\boldsymbol{K_{i,16}}}\right)^{\boldsymbol{h_{16}}}\right)}{[Fps1P]_0}$	
k_{16_7}	$\frac{\boldsymbol{k_{15}} \cdot 0.5 \cdot [Fps1]_0 \left(1 + \left(\frac{[Hog1PP]_0}{\boldsymbol{K_{i,16}}}\right)^{\boldsymbol{h_{16}}}\right)}{[Fps1P]_0}$	
k_{16_8}	$\frac{\boldsymbol{k_{15}} \cdot [Fps1]_0 \left(1 + \left(\frac{[Hog1PP]_0}{\boldsymbol{K_{i,16}}}\right)^{\boldsymbol{h_{16}}}\right)}{[Fps1P]_0}$	

Table S6: Constants used in the models.

Parameter	Value	Description
R [J/mol/K]	8.314	Gas constant.
T [K]	303.15	Temperature, corresponds to 30°C.
mol	$6.022 \cdot 10^{23}$	Mole number.
θ	0.93	Osmotic coefficient for salt.
f_{c2p}	10^{-9}	Factor converting concentrations in M to pressures in MPa.
t_m [s]	10	Mixing time [s] of salt in the medium.
L_p [µm/Mpa/s]	0.013	Hydraulic conductivity (estimate from data from (Eriksson, et al., 2007)).
P_0 [MPa]	0.61	Initial turgor pressure (Schaber, et al., 2010)
ε	14.3	Membrane rigidity (Schaber, et al., 2010)
$f_{\min}$	0.41	Minimal cell volume (as fraction of total) (Schaber, et al., 2010)
f_n	0.8	Fraction of activated Hog1 molecule in the nucleous upon maximal activation.
c_0^e [µM]	260000	Initial osmolarity of the medium (Schaber, et

		al., 2010)
V_0 [fl]	50	Initial total cell volume.
$Pbs2_t$ [µM]	0.1216	$2160 f_{n2\mu M}$: molecule numbers from http://yeastgfp.yeastgenome.org/
$Sho1_t$ [µM]	0.1313	$2330 f_{n2\mu M}$: molecule numbers from http://yeastgfp.yeastgenome.org/
$Hog1_t$ [µM]	0.3821	$6788 f_{n2\mu M}$: molecule numbers from http://yeastgfp.yeastgenome.org/
$Fps1_t$ [µM]	0.051	$907 f_{n2\mu M}$: molecule numbers from http://yeastgfp.yeastgenome.org/
$h_{TurgorActiv}$	2	Hill parameter of the turgor-activate Fps1 closure.

Table S7: Estimated parameter values ± asymptotic standard deviation for the best approximating model (Nr. 22).

Parameter	**Value**	**Description**
kHog1dephos	1.78587 ± 1.55E-01	Rate constant for reaction v_6 and v_8 [1/µM /s]
kHog1phos1	42.6397 ± 1.47E+01	Rate constant for reaction v_5 and v_7 (Sho1 branch) [1/µM /s]
kHog1phos2	48.0004 ±4.30E+01	Rate constant for reaction v_5 and v_7 (Sln1 branch) [1/µM /s]
(v1_fb).Ki	0.00940584 ± 2.10E-03	Inhibition constant for reaction v_1 [µM]
(v1_fb).h	0.345701 ± 1.27E-02	Hill constant for reaction v_1 [–]
(v1_fb).k	0.075474 ± 2.66E-02	Rate constant for reaction v_1 [1 /s]
(v2).k	0.607124 ± 2.44E-02	Rate constant for reaction v_2 [1/µM/s]
(v3_fb).Ki	0.297524 ± 1.11E-02	Inhibition constant for reaction v_3 [µM]
(v3_fb).h	2.0793 ± 4.58E-02	Hill constant for reaction v_3 [–]
(v3_fb).k	0.00459138 ± 4.24E-03	Rate constant for reaction v_3 [1/s]
(v4).k1	0.00226722 ± 4.01E-05	Rate constant for reaction v_4 [1/s]
(v9).Km	0.506878 ± 5.42E-03	Michaelis-Menten constant for reaction v_9 [µM]
(v9).k	18.1824 ± 4.63E+01	Rate constant for reaction v_9 [µM /s]
(v11).k	9.07E-05 ± 8.19E-07	Rate constant for reaction v_{11} [1/s]
(v13).Km	0.420741 ± 5.22E-03	Michaelis-Menten constant for reaction v_{13} [µM]

(v13).k1	680.818 ± 5.13E+00	Rate constant for reaction v_{13} (Gpd1 influence) [μM/s]
(v13).k2	46.8363 ± 1.78E+00	Rate constant for reaction v_{13} (Hog1 influence) [1/μM]
(v15_5).k	0.00529124 ±3.81E-04	Rate constant for reaction v_{15_5} [1/s]
(v16_6).Ki	0.0811033 ± 9.86E-03	Inhibition constant for reaction v_{16_6} [μM]
(v16_6).h	0.628719 ± 3.02E-02	Hill constant for reaction v_{16_6} [–]

Table S8: First ten candidate models according to AICc using both fitted and predicted SSR including models with oscillations.

		Candidate Models Mechanisms											
Rank	**Model Nr.**	**Fps1 opening**	**Fps1 closure**	**Fps1 degradation**	**Branch feedback**	**Glycerol production**	**Osccilations**	***n***	***k***	***SSR***	***AICc***	**Akaike weight**	**cutoff**
1	22	H	T	-	B	H+G	-	515	20	547.4	1532.9	0.56	OK
2	30	H	T	H	B	H+G	-	515	21	546.2	1533.8	0.36	OK
3	170	H	A	P	B	G	++	515	21	550.4	1537.7	0.05	OK
4	78	H	T	P	B	H+G	-	515	21	551.9	1539.2	0.02	-
5	126	H	T	H	B	G	++	515	20	555.7	1540.7	0.01	-
6	174	H	T	P	B	G	++	515	20	562.8	1547.2	0.00	-
7	17	-	A	-	B	H+G	-	515	19	584.0	1564.3	0.00	-
8	32	H + T	T	H	B	H+G	++	515	21	581.7	1566.2	0.00	-
9	128	H + T	T	H	B	G	++	515	20	586.9	1568.8	0.00	-
10	24	H + T	T	-	B	H+G	-	515	20	588.3	1570.0	0.00	-

AICc: corrected Akaike information criterion, *SSR*: sum of squared residuals, *n* number of data points, *k* number of fitted parameters. Candidate Model Mechanisms: H - Hog1 dependent, T - Turgor dependent, A - Area dependent, P – Protein dependent, G – Gpd1 dependent, B – feedback on both branches. -: None, ++ oscillations or damped oscillation with more than 5 clearly visible peaks.

Table S9: First ten candidate models according to AICc using only fitted SSR excluding models with oscillations.

Rank	Model Nr.	Candidate Model Mechanisms: Fps1 opening	Fps1 closure	Fps1 degradation	Branch feedback	Glycerol production	N	K	SSR	AICc	Akaike weight	cutoff
1	22	H	T	-	B	H+G	390	20	426.9	1184.3	0.51	OK
2	78	H	T	P	B	H+G	390	21	425.0	1184.8	0.39	OK
3	30	H	T	H	B	H+G	390	21	428.2	1187.7	0.09	OK
4	17	-	A	-	B	H+G	390	19	455.3	1207.2	0.00	-
5	24	H + T	T	-	B	H+G	390	20	457.1	1210.9	0.00	-
6	23	T	T	-	B	H+G	390	18	463.7	1212.1	0.00	-
7	18	H	A	-	B	H+G	390	21	460.0	1215.7	0.00	-
8	20	H + T	A	-	B	H+G	390	21	460.2	1215.9	0.00	-
9	75	T	A	P	B	H+G	390	20	467.7	1219.9	0.00	-
10	19	T	A	-	B	H+G	390	19	426.9	1184.3	0.00	-

AICc: corrected Akaike information criterion, *SSR*: sum of squared residuals, *n* number of data points, *k* number of fitted parameters. Candidate Model Mechanisms: H - Hog1 dependent, T - Turgor dependent, A - Area dependent, P – Protein dependent, G – Gpd1 dependent, B – feedback on both branches.

Table S10: First ten candidate models according to AICc using using both fitted and predicted SSR excluding models with oscillations.

Rank	Model Nr.	Candidate Model Mechanisms: Fps1 opening	Fps1 closure	Fps1 degradation	Branch feedback	Glycerol production	N	K	SSR	AICc	Akaike weight	cutoff
1	22	H	T	-	B	H+G	515	20	547.4	1534.6	0.61	OK
2	30	H	T	H	B	H+G	515	21	546.2	1535.6	0.36	OK
3	78	H	T	P	B	H+G	515	21	551.9	1541.0	0.02	-
4	17	-	A	-	B	H+G	515	19	584.0	1565.8	0.00	-
5	24	H + T	T	-	B	H+G	515	20	588.3	1571.7	0.00	-
6	23	T	T	-	B	H+G	515	18	595.7	1573.9	0.00	-
7	86	H	T	P	S	H+G	515	19	599.6	1579.4	0.00	-
8	18	H	A	-	B	H+G	515	21	596.3	1580.9	0.00	-
9	20	H + T	A	-	B	H+G	515	21	596.9	1581.4	0.00	-
10	81	-	A	P	S	H+G	515	18	547.4	1534.6	0.00	-

AICc: corrected Akaike information criterion, *SSR*: sum of squared residuals, *n* number of data points, *k* number of fitted parameters. Candidate Model Mechanisms: H - Hog1 dependent, T - Turgor dependent, A - Area dependent, P – Protein dependent, G – Gpd1 dependent, B – feedback on both branches, S – feedback on Sln1-branch only.

2 Saturation and inhibition kinetics

In table S4 the kinetics of all rate reactions used in the model are listed. For most reactions we assumed simple mass actions. This was mainly due to the lack of more detailed information about the involved kinetics and due to our guiding principle of parsimony. However, in several cases saturation and inhibition kinetics were used, whose rationale are described here in more detail.

In the course of the model development we realised that assuming simple mass action kinetics in reactions v_9 and v_{13} could not explain the data well. However, using a simple saturation kinetic gave good results implying that saturation seems to be an important feature of these reactions (see also Table S11). Therefore, in reactions v_9 and v_{13} we use a saturation kinetic in the form v=k*$M/(K_m+M)$, where v is the reaction velocity [µM/s], k [µM/s] is the rate constant equivalent to the maximal reaction velocity, K_m [µM] is a constant equal to the half saturation concentration of M [µM], and M is a modifier. Note that the kinetic rate law has the form the Michaelis-Menten rate law, but it is not a Michaelis-Menten reaction, because M is not a substrate but a modifier and, hence, is not consumed by this reaction. Such a formulation is inspired by the assumption that transcription and glycerol production cannot be up-regulated arbitrarily as a function of the modifier, because there will be limiting factors or processes, which are not explicitly considered here. In the case of v_9 this might be promotor accessibility, and in the case of v_{13} this might be other metabolic steps preceding glycerol synthesis or co-factors, like NADH.

Mechanistically, such a formulation can easily be derived by assuming the following simplistic reactions and corresponding ordinary differential equations, for details see (Alon, 2007):

$$n[M] + [C] \leftrightarrow [nMC]$$

$$[nMC] \rightarrow [G] + [nMC]$$

with

$$\frac{d[nMC]}{dt} = k_{on}[M]^n[C] - k_{off}[nMC]$$

$$\frac{d[G]}{dt} = \frac{k}{C_t}[nMC]$$

where C is a component that may become limiting, n is an integer indicating the amount of molecules of M that can bind C, assuming that either n or none molecules of M are bound to C and C_t=[C]+ [nMC]. Further assuming that the first reaction is in equilibrium compared to the second reaction, it can be derived that

$$\frac{d[G]}{dt} = \frac{k[M]^n}{K_m^n+[M]^n} \ ,$$

with $K_m = \sqrt[n]{\frac{k_{on}}{k_{off}}}$.

In the cases of reaction v_9 and v_{13} we can argue that [*Hog1PP*] or [*Protein*], respectively, can be assumed to bind to some other components, which in turn acts as a modifier to the respective reaction. In case of v_9 this would be, e.g., the promotor of the gene, and in case of v_{13} this would be, e.g., the co-factor NADH. Moreover, we set n=1 for simplicity.

For reaction v_{13} we additionally included [*Hog1PP*] as a potential modifier. The mechanisms how [*Hog1PP*] increases the glycerol synthesis rate is still unclear, even though there are some indications (see main text and (Dihazi, et al., 2004)). For this reason we introduced a simple heuristic approach assuming that the effective modifier concentration can be increased by [*Hog1PP*], such that $[M] = [Protein] \cdot (1 + \boldsymbol{k_{13\_2}} \cdot [Hog1PP])$. There are many possibilities to include [*Hog1PP*] as an additional modifier. Because this reaction and especially the role of [*Hog1PP*] turned out to be important, we tested several possibilities of including [*Hog1PP*] with only one additional parameter and a saturation kinetic. The kinetic used in the final models turned out to be best supported by data. In the next section, we provide some details about this comparison (Tables S11, S12).

For the inhibition kinetics a similar mechanism as above can be assumed (Alon, 2007) All inhibition kinetics are composed by a mass action term for the actual reaction to be inhibited, which is multiplied by the term $\frac{1}{1+\left(M/K_i\right)^n}$. Such a term can be derived assuming the following reactions and corresponding ordinary differential equations, for details see (Alon, 2007):

$$n[M] + [C] \leftrightarrow [nMC]$$

$$[C] \rightarrow [G] + [C]$$

with

$$\frac{d[nMC]}{dt} = k_{on}[M]^n[C] - k_{off}[nMC]$$

$$\frac{d[G]}{dt} = \frac{k}{C_t}[C]$$

where C is a component that may become limiting, n is an integer indicating the amount of molecules of M that can bind C, assuming that either n or none molecules of M are bound to C and C_t=[C]+ [nMC]. Further assuming that the first reaction is in equilibrium compared to the second reaction, it can be derived that

$$\frac{d[G]}{dt} = \frac{k}{1+\left(\frac{[M]}{K_i}\right)^n} ,$$

with $K_i = \sqrt[n]{\frac{k_{on}}{k_{off}}}$.

3 Frequency Response

To study the frequency response of the best approximating model Nr. 22, we stimulated the model with a series of consecutive shocks of 0.2 M NaCl with periods of P_0 = 2 minutes to P_0 = 64 minutes until the amplitude of the response remained constant (Figure S1). One stimulation period is equally divided into two parts, i.e with and without shock as in Mettetal et al. (2008).

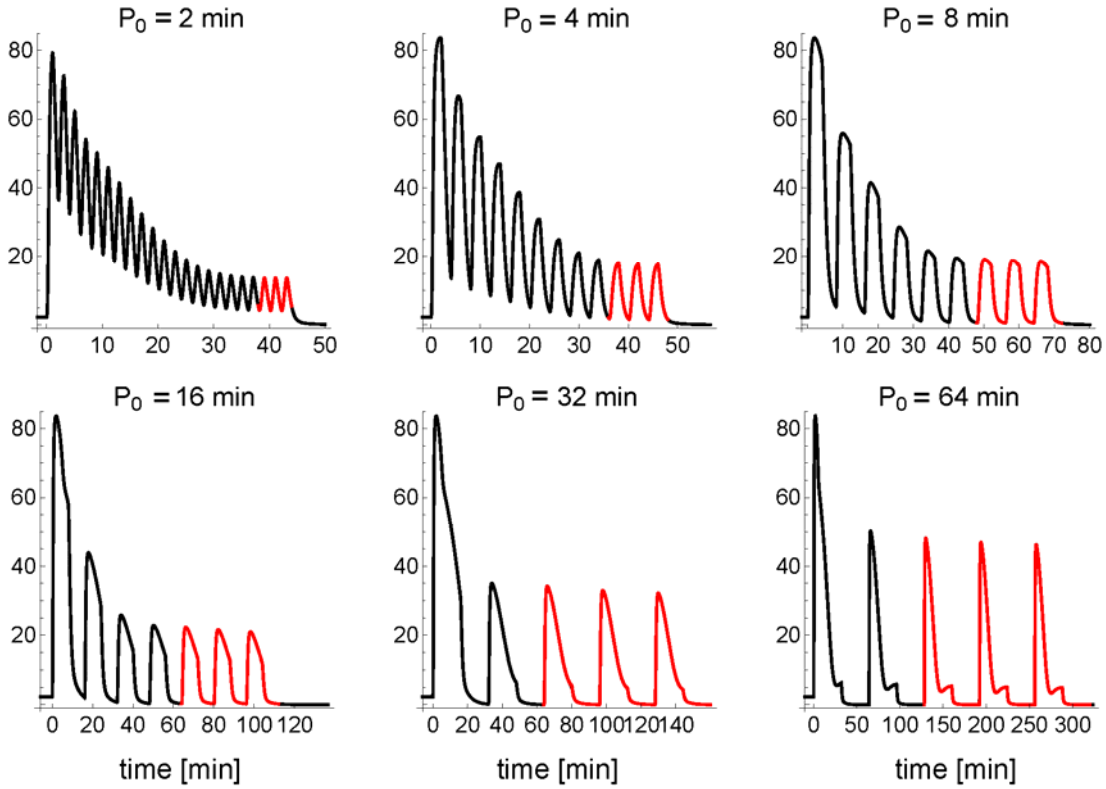

Figure S1: Simulated Hog1 phosphorylation for consecutive shocks of 0.2M of the indicated periods P_0. The parts of the simulations marked in red were taken for the calculation of the response amplitude $A(\omega)$.

When a steady-state response was reached, i.e. when the amplitude of the response $A(\omega)$ as a function of the stimulation frequency $\omega = 2\pi/P_0$ remained constant, the response of the last three complete periods (red lines in Figure S1 and S2) was taken to calculate $A(\omega)$ from the corresponding Fourier coefficient $F(\omega)$.

$$F(\omega) = 2\int_{nP_0}^{(n+m)P_0} \frac{e^{-i\omega t}S(t)}{mP_0}\,dt$$

where n is the starting period for the calculation after start of the experiment, m is the number of periods taken for the calculation (marked in red in Figures S1 and S2) and $S(t)$ is the respective simulation (Figure S1) or interpolated data (Figure S2). The amplitude of the response is then defined as $A(\omega) = |F(\omega)|$ (Mettetal, et al., 2008).

We re-calculated the response amplitude of Hog1 nuclear localisation from data published in the Supplementary Material from Mettetal et al (2008), which we digitized from Figure S2 therein (Figure S2).

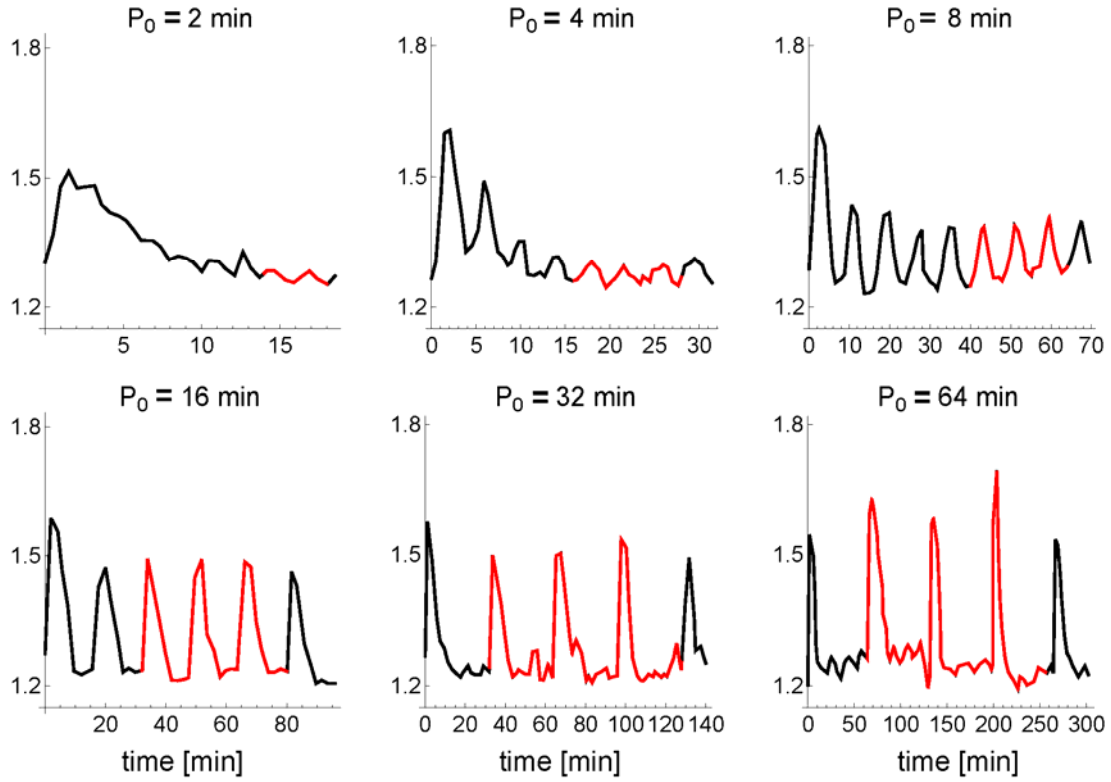

Figure S2: Measured Hog1 nuclear localisation after consecutive shocks of 0.2M of the indicated periods P_0 (data digitised from Figure S2 in Mettetal et *al*. (2009)). The parts of the simulations marked in red were taken for the calculation of the response amplitude $A(\omega)$.

In Figure S3 the resulting Bode plots for the simulation and the re-analysed data from Mettetal et al. (2008) are shown. For both the simulations and the data, we observe an increasing response amplitude $A(\omega)$ with decreasing frequency ω. Such behaviour has also been observed in another study and described as a low-pass filter characteristic (Hersen, et al., 2008). We assume that simulation and measurements are comparable, because Hog1 nuclear localisation and Hog1 phosphorylation are highly correlated.

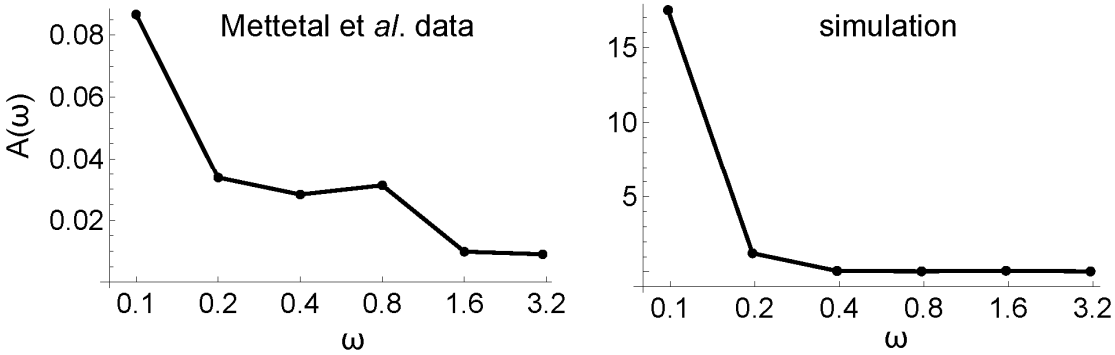

Figure S3: Response amplitude $A(\omega)$ vs. frequency ω for the simulation (Figure S1) and the re-analysed data from Mettetal et al. (2009) (Figure S2). Note the for the data (left panel) $A(\omega)$ of Hog1 nuclear localisation is shown, whereas for the simulation (right panel) $A(\omega)$ of Hog1 phosphorylation is shown.

4 Model sensitivities

Kinetic rate laws for reaction v_{13}

It turned out that for the best approximating model reaction v_{13} had important implications, especially about the role of Hog1 in osmo-adapation. The mechanism of how Hog1 modifies glycerol synthesis is still elusive, even though there are some indications (see main text, (Dihazi, et al., 2004)) and it is probably indirect. Therefore, we tested several possible kinetic rate laws for reaction v_{13} using the three best approximating models Nr. 22, Nr. 78 and Nr. 30 (Tables S9, S10) under the constraint that a saturation kinetic and only one additional parameter should be involved. Tested possible heuristic approachs are listed in Table S11.

Table S11: Kinetic rates law tested for reaction v_{13}

Name	Rate law	Description
K1	$\frac{\boldsymbol{k_{13\_1}}[Protein](1+\boldsymbol{k_{13\_2}}\cdot[Hog1PP])}{\boldsymbol{Km_{13}}+[Protein](1+\boldsymbol{k_{13\_2}}\cdot[Hog1PP])}$	Modifier is enhanced by [*Hog1PP*] in a bilinear fashion
K2	$\frac{\boldsymbol{k_{13\_1}}([Protein]+\boldsymbol{k_{13\_2}}[Hog1PP])}{\boldsymbol{Km_{13}}+[Protein]+\boldsymbol{k_{13\_2}}[Hog1PP]}$	Modifier is enhanced by [*Hog1PP*] in a linear fashion
K3	$\frac{(\boldsymbol{k_{13\_1}}+\boldsymbol{k_{13\_2}}[Hog1PP])[Protein]}{\boldsymbol{Km_{13}}+[Protein]}$	Maximal reaction velocity is modified by [*Hog1PP*]
K4	$\frac{\boldsymbol{k_{13\_1}}[Protein]}{\boldsymbol{Km_{13}}+[Protein]}+\boldsymbol{k_{13\_2}}[Protein][Hog1PP]$	[*Hog1PP*] modifies reaction velocity by mass action
K5	$\boldsymbol{k_{13\_1}}[Protein]+\frac{\boldsymbol{k_{13\_2}}[Protein][Hog1PP]}{\boldsymbol{Km_{13}}+[Hog1PP]}$	[*Hog1PP*] modifies reaction velocity by saturation kinetic
K6	$\boldsymbol{k_{13\_1}}[Protein]+\boldsymbol{k_{13\_2}}[Protein][Hog1PP]$	Mass action only

Each of the three best approximating models were implemented with the different possible kinetics and refitted as the original models and ranked. The results of the model discrimination disregarding oscillating models are listed in Table S12.

Table S12: Model discrimination analysis for different kinetic rate laws for reaction v_{13} using the three best approximating models Nr. 22, 78 and 30.

Rank	Model	Candidate Mechanisms for Reaction v_{13} in Models Nr. 22, Nr. 78 and Nr. 30 (Table S11)	N	K	SSR	AICc	Akaike weight	cutoff
1	22	K1	390	20	426.9	1184.3	1.00	OK
2	78	K1	390	21	425.0	1184.8	0.77	OK
3	30	K1	390	21	428.2	1187.7	0.18	OK
4	78	K2	390	21	432.3	1191.4	0.03	NO
5	22	K2	390	20	442.8	1198.6	0.00	NO

6	22	K6	390	19	535.9	1270.8	0.00	NO
7	30	K6	390	20	691.2	1372.2	0.00	NO
8	78	K6	390	20	693.0	1373.2	0.00	NO
9	78	K5	390	21	1007.3	1521.4	0.00	NO
10	22	K4	390	20	1518.5	1679.2	0.00	NO

AICc: corrected Akaike information criterion, *SSR*: sum of squared residuals, *n* number of data points, *k* number of fitted parameters.

The kinetic rate law used in the final version of the model (K1) is best supported by the data.

Parameter sensitivities

We calculated relative sensitivities *S* as

$$S = \frac{\frac{\Delta O}{O}}{\frac{\Delta p}{p}},$$

where $\Delta O/O$ is the relative change of the 95% volume adaptation time upon 0.4 M NaCl osmotic shock, i.e. the time the cell needs to recover 95% of its initial volume, and $\Delta p/p$ is the relative change in parameter or initial condition, compared to the initial state, respectively.

In Table S11 we list the maximum of the absolute value of *S*, where we multiplied and divided the initial conditions by 2 and the parameters by 5, respectively.

Table S13: Maximum of absolute sensitivities of the 95% volume adaptation times upon 0.4 M NaCl osmotic shock .

Initial Condition	***S***	**Parameter**	***S***
$Sho1_0$	0.02	kHog1dephos	0.18
$Pbs2_t$	0.15	kHog1phos1	0.19
$Hog1_t$	0.16	kHog1phos2	0.04
$Hog1PP_0$	0.16	(v1_fb).Ki	0.05
$Phosphatase_0$	0.1	(v1_fb).h	0.07
RNA_0	0.11	(v1_fb).k	0.18
$Protein_0$	0.07	(v2).k	0.10
$Glyin_0$	0.22	(v3_fb).Ki	0.05
$Fps1_t$	0.00	(v3_fb).h	0.02
P_0	2.38	(v3_fb).k	0.04
ε	0.28	(v4).k1	0.04

V_0	0.00	(v9).Km	0.18
		(v9).k	0.00
		(v11).k	0.26
		(v13).Km	0.93
		(v13).k1	2.38
		(v13).k2	0.79
		(v15_5).k	0.28
		(v16_6).Ki	0.11
		(v16_6).h	0.36

5 Likelihood profiles

In order to address identifiability of the parameters we calculated likelihood profiles for each fitted parameter, respectively (Raue, et al., 2009; Schaber 2012; Schaber and Klipp, 2011). The likelihood profile $LP(p_i)$ for each parameter $\hat{p}_i$ (i=1,…,m) is defined as

$$LP(p_i) = \min_{p_{j\neq i}}(SSR(p))$$

i.e. re-optimizing the objective function value $SSR(p)$ with respect to all parameters $p_{j\neq i}$ for defined values of p_i in a neighbourhood of the original estimated parameter value $\hat{p}_i$ (Table S7). For simplicity, we varied the p_i in 20 logarithmic steps in the range $\frac{\hat{p}_i}{10} \leq p_i \leq 10\hat{p}_i$, respectively. Only the range for parameter (v3_fb).k3 and (v16_6).h16 we had to extend more in order to reach the confidence limit. For each step $SSR(p)$ was re-optimised varying all parameters $p_{j\neq i}$ with a Hookes and Jeeves algorithm with 10 iteration steps.

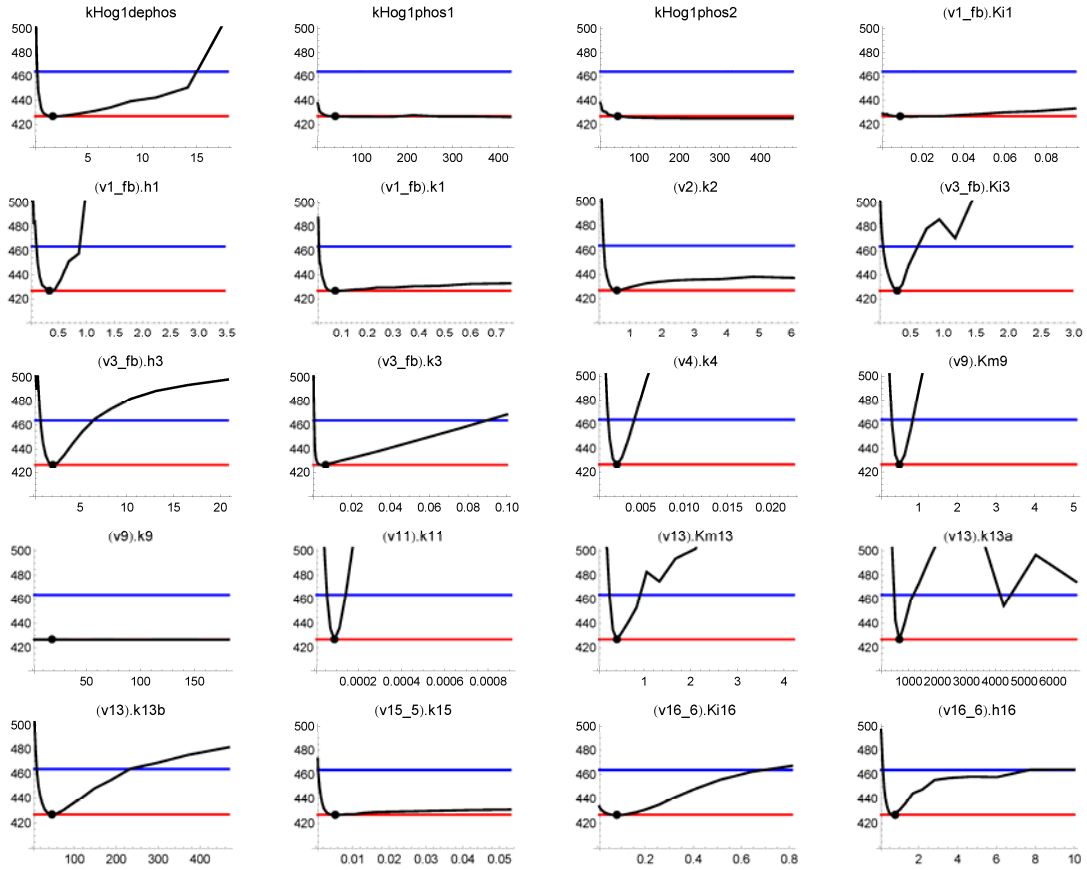

Figure S4: Likelihood profiles for the fitted parameters of Model 22 (Table S7). Black line: Re-fitted *SSR* for the parameter indicated in the plot label. Black point: original parameter value with the original *SSR*. Red line: original *SSR* of Model 22. Blue line: 95% confidence level, according to the approximate ellipsoidal 100(1- α)% confidence region for $\hat{p}$: $P_{CR} = \left\{ p : SSR(p) \le SSR(\hat{p}) \left(1 + \frac{m}{n-m} F^{\alpha}_{m,n-m} \right) \right\}$. $F^{\alpha}_{m,n-m}$ is the upper α-critical value for the $F_{m,n-m}$ -distribution, where *m* is the number of parameters and *n* the number of data points (Seber and Wild, 2003).

6 Adaptation times

Table S14: Mean adaptation times [min] ± standard deviation for 500 Monte-Carlo simulations.

Condition (adaptation time)	wt	Sln1 branch	Sho1 branch
0.05 M NaCl (99%)	8.0 ± 2.5	9.8 ± 4.0	23.8 ± 6.9
0.1 M NaCl (99%)	9.3 ± 2.3	11.1 ± 3.7	22.3 ± 6.5
0.2 M NaCl (95%)	9.6 ± 2.0	10.7 ± 2.8	14.4 ± 4.1
0.4 M NaCl (95%)	26.6 ± 3.8	28.1 ± 4.4	29.5 ± 4.1

7 The simplified HOG model

7.1 Ordinary differential equation system

$$\frac{d[Hog1PP]}{dt} = k\max(E_0 + [NaCl] - [Glycerol] + T_0, 0)\frac{(H_t - [Hog1PP])}{1 + \left(\frac{[Hog1PP]}{K_i}\right)^n} - k_2[Hog1PP]$$

$$\frac{d[RNA]}{dt} = k[Hog1PP] - k_4[RNA]$$

$$\frac{d[Protein]}{dt} = k[RNA] - k_6[Protein]$$

$$\frac{d[Glycerol]}{dt} = k[Protein][Hog1PP] - k_8[Glycerol]$$

The components marked in red indicate the optional feedbacks.

7.2 Initial conditions and derived quantities

The simplified HOG model should also start from a non-zero steady-state, as the full model. Therefore, we set to initial values of the model to arbitrary values of with T_0=0.02, $[Hog1]_0$=0.05, $[RNA]_0$=0.01, $[P]_0$=0.03, E_0=$[Glycerol]_0$=0.3, H_t=1, k=0.1, $[NaCl]$=0., K_i=0.1,n=2.

Using the steady state assumption and the parameter k, we can thus set the degradation rates:

$$k_2 = \frac{k(E_0 - [Glycerol]_0 + T_0)\frac{(H_t - [Hog1PP]_0)}{1+\left(\frac{[Hog1PP]_0}{K_i}\right)^n}}{[Hog1PP]_0}$$

$$k_4 = \frac{k[Hog1PP]_0}{[RNA]_0}$$

$$k_6 = \frac{k[RNA]_0}{[Protein]_0}$$

$$k_8 = \frac{k[Protein]_0[Hog1PP]_0}{[Glycerol]_0}$$

7.3 Bifurcation Diagrams

A computational analysis of the eigenvalues of the Jacobian matrix of the simplified HOG model showed that when the real part of the maximum eigenvalue changes from negative to positive, i.e. from white squares to grey squares in Figure 9, there is a single pair of complex conjugated eigenvalues crossing the imaginary axis and the

remaining two eigenvalues remain negative. This is the hallmark of a Hopf-bifurcation giving rise to, in our case, stable oscillations. We illustrate this by plotting bifurcation diagrams of *Hog1PP* equilibria as a function of T_0 for selected values of *NaCl* (Figure S5).

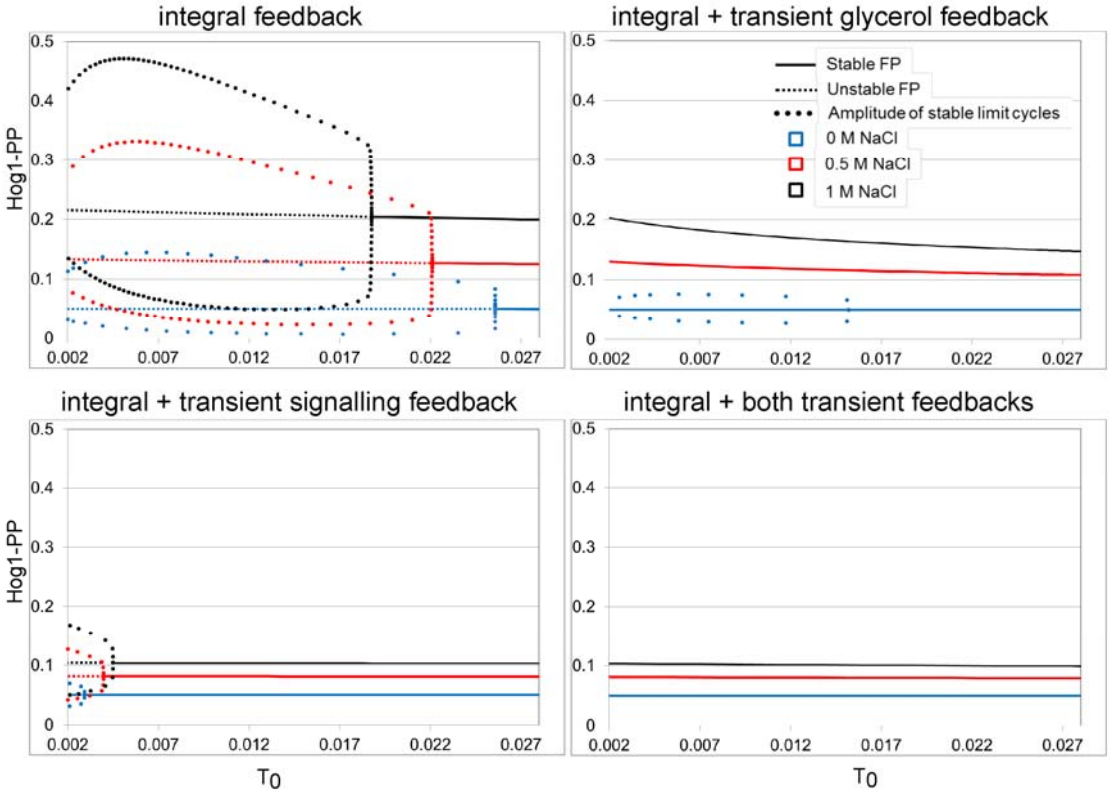

Figure S5: Bifurcation diagrams of the simplified HOG model including different feedbacks. The abscissa shows T_0 and the ordinate shows equilibria of *Hog1PP*. Solid lines indicate stable equilibria, dotted lines indicate unstable eqilibria, solid circles indicate the amplitude of stable oscillations. The colours indicate different NaCl conditions: Blue: 0 M NaCl, red: 0.5M NaCl, balck: 1 M NaCl. See also Figure 9 in the main text.

Strictly speaking, the oscillations are a consequence of a Hopf-bifurkation only near the bifurcation point as long as the signal $E_0 + [NaCl] - [Glycerol] + T_0 > 0$ for the whole trajectory. Due to the maximum function in the signal formulation, a different situation arises as soon as $E_0 + [NaCl] - [Glycerol] + T_0 \leq 0$. In this situation, the model changes and oscillations are a consequence of a different mechanism, but they persist as can be seen in the bifurcation diagram. In order to obtain oscillations as a consequence of a Hopf-bifurcation over the whole parameter range it suffices to have a smoothly differentiable function $f(E_0 + [NaCl] - [Glycerol] + T_0) > 0$ as input signal.

8 The model correctly predicts effect of wild type and single branch inhibition

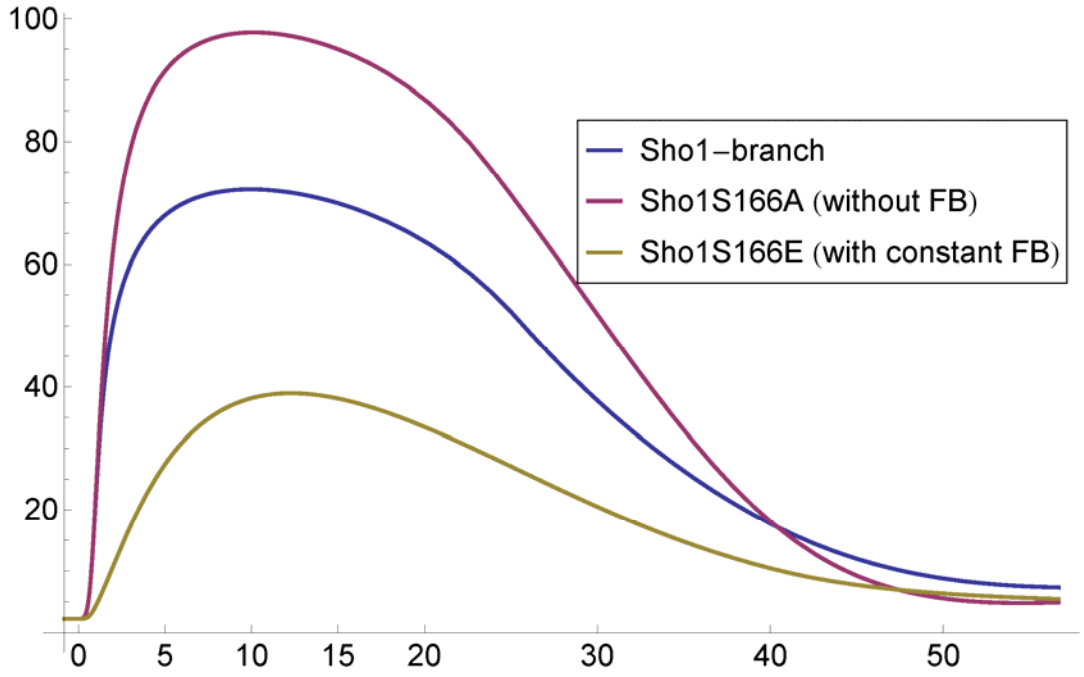

Figure S6: Simulated Sho1 branch mutants mimicking experiments done in Hao et al. (2007), Compare to Figure 5B therein. FB denotes feedback.

9 Direct non-transcriptional modification of glycerol production by Hog1 is the main mechanism responsible for Hog1 phosphorylation upon inhibition of Hog1 activity

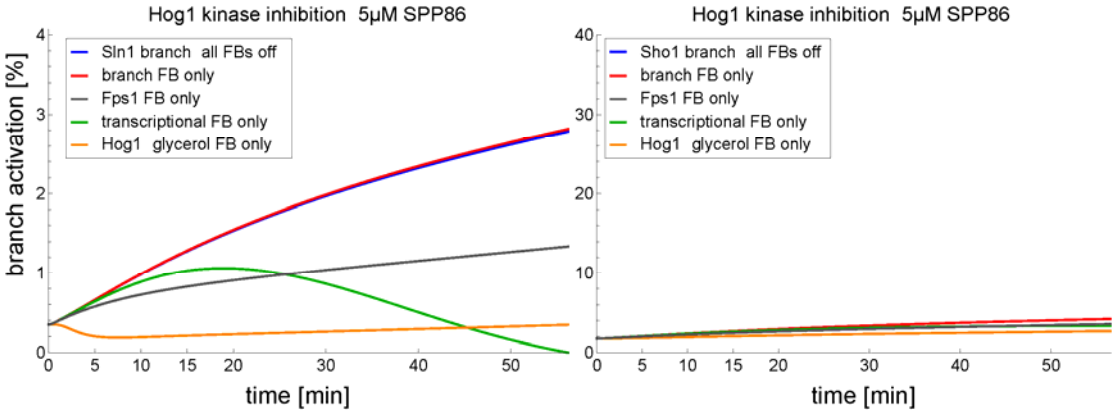

Figure S7: Simulated branch activations where only one of several feedback mechanisms (FB) is active at a time for the Sln1 branch and the Sho1 branch, respectively.

10 The two branches compete for Pbs2, but are partly additive

The best approximating model (Nr. 22), as most of the other fitted top 10 models, is able to predict the wild type Hog1 activation data (Figure 3A) even though only the single branch data was used to parameterise the model. This is an interesting result as the single branch mutants do not have to compete for Pbs2, whereas the wild type does. The possible outcome could have been everything in the range from total competition, i.e each single branch using all of the available Pbs2, to completely additive, i.e. each branch is activating a small portion of available Pbs2, which is additive in the wild type. The prediction is a mixture of both. Both single branches only activate a small portions of the available Pbs2 (Supplementary Figure S8 and S9), however, these portion are only to a small part additive. The additive effect of Pbs2 activation translates to Hog1 activation for low stress. For low stress, i.e. lower than 0.1 M NaCl, Hog1 activation of the wild type is more pronounced than for both branches alone (Supplementary Figure S8). For larger osmotic shocks, i.e. larger than 0.4M NaCl, this effect vanishes for Hog1 maximal amplitude due to saturation effects (Supplementary Figure S9).

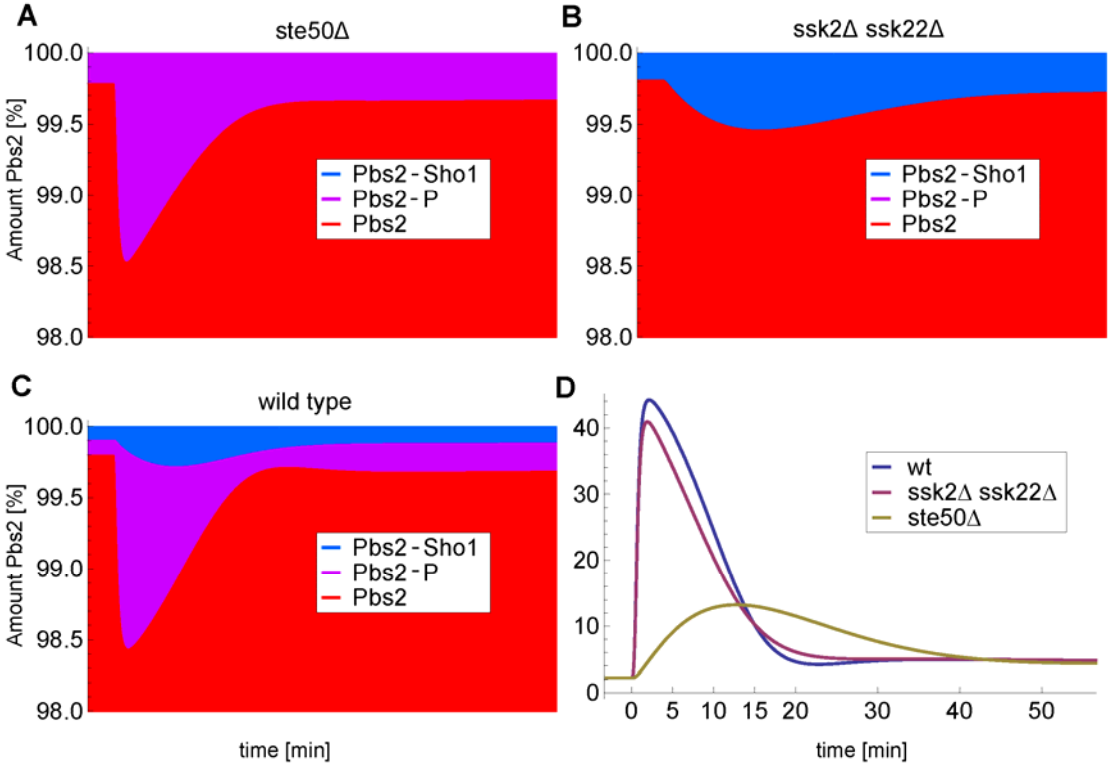

Figure S8: Pbs2 distribuiton and Hog1 activation for both branches and the wild type for 0.1 M NaCl. **A**: Pbs2 distribuiton Sln1-branch (ste50Δ) simulation. **B**: Pbs2 distribuiton Sho1 (Ssk2Δ Ssk22Δ) branch simulation. **C**: Pbs2 distribution wild type simulation.**D**: Activation Hog1 simulation for both branches and the wild type for 0.1 M NaCl

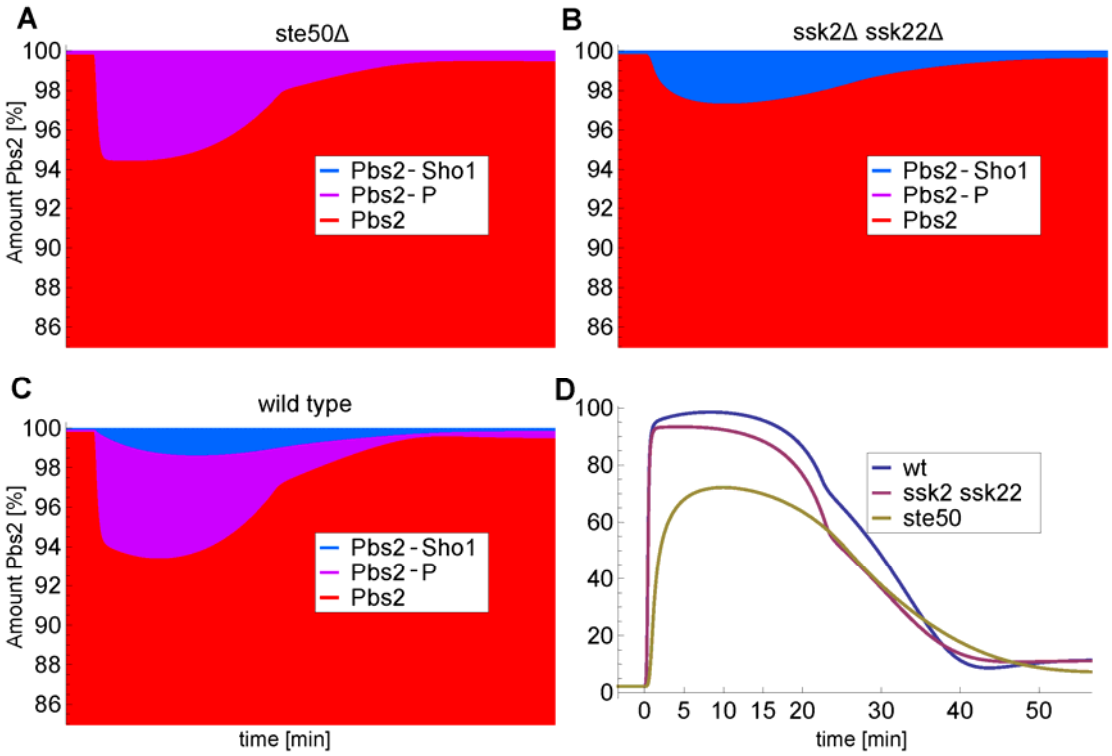

Figure S9: Pbs2 distribuiton and Hog1 activation for both branches and the wild type for 0.4 M NaCl. **A**: Pbs2 distribuiton Sln1-branch (ste50Δ) simulation. **B**: Pbs2 distribuiton Sho1 (Ssk2Δ Ssk22Δ) branch simulation. **C**: Pbs2 distribution wild type simulation.**D**: Activated Hog1 simulation for both branches and the wild type for 0.4 M NaCl

11 There is no perfect adaptation at the level of Hog1 phosphorylation

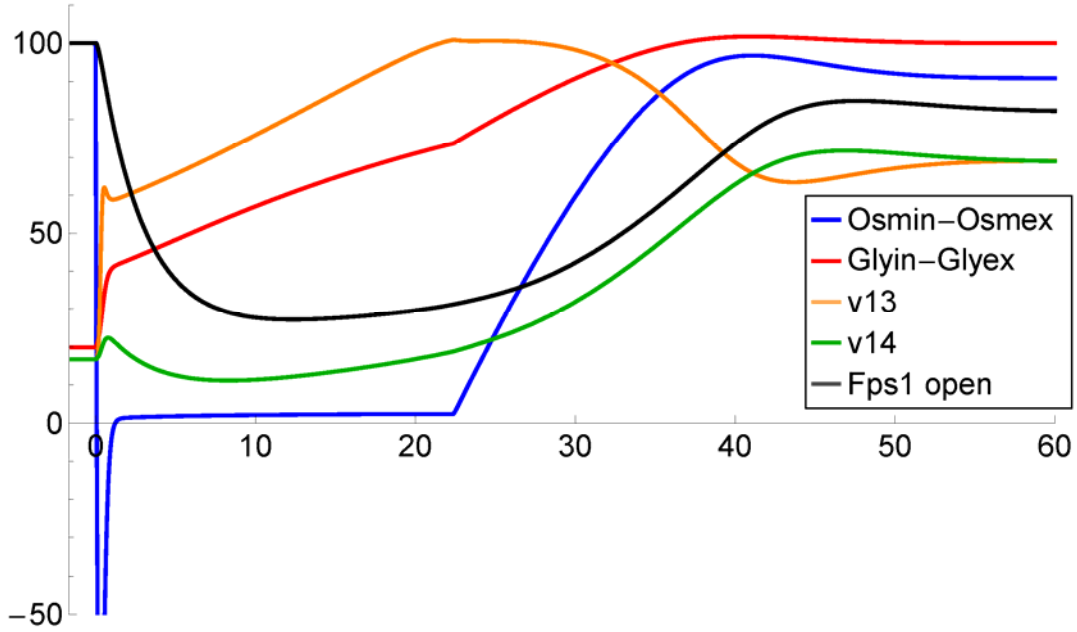

Figure S10: Dynamics of gradients and flows characterising osmolarity and glycerol in yeast upon an osmotic shock of 0.4 M NaCl scaled to maximum levels, respectively.

In the model, after adaptation the difference between internal and external osmolarity, which is equilibrated by turgor (Schaber, et al., 2010; Schaber and Klipp, 2008), returns almost to its initial values (Supplementary Figure S10, blue line). This, of course, is a prerequisite of volume adaptation. However, the glycerol flux across the membrane (see reaction v_{14} and Supplementary Material), which is proportional to the difference between internal and external glycerol, does not return to pre-shock levels. The difference between internal and external glycerol increases after adaptation (Supplementary Figure S10, red line), which is mainly due to the fact that in the model internal osmolarity is predominantly regulated by glycerol, whereas in the external medium leaking glycerol is drastically diluted. Accordingly, the simulated outflow increases, which in turn has to be balanced by an increase in the steady-state production (Supplementary Figure S10, orange and green lines). The data best supports a model in which glycerol production is a function of activated Hog1, both directly and indirectly by elevated protein production (see Figure 1 in the main text). Thus, the model suggests that elevated glycerol production can only be maintained by an elevated Hog1 activity. In a recent paper it was shown that perfect adaptation in terms of Hog1 activity can theoretically be achieved by maintaining the Fps1 channel in a closed state after adaptation (Schaber, et al., 2010). Here, however, a model was selected that assumes channel closure to be a function of turgor and Hog1 activity. Returning to almost the initial Fps1 state after adaptation (Supplementary Figure S10,

black line) renders the systems more flexible to react to subsequent shocks, at the cost of an elevated glycerol efflux that has to maintained.

12 References

Alon, U. (2007) *An Introduction to Systems Biology*. Mathematical and Computational Biology Series. Chapman and Hall/CRC, Boca Raton.

Dihazi, H., Kessler, R. and Eschrich, K. (2004) High osmolarity glycerol (HOG) pathway-induced phosphorylation and activation of 6-phosphofructo-2-kinase are essential for glycerol accumulation and yeast cell proliferation under hyperosmotic stress, *J Biol Chem*, 279, 23961-23968. Epub 22004 Mar 23922.

Eriksson, E., *et al.* (2007) A microfluidic system in combination with optical tweezers for analyzing rapid and reversible cytological alterations in single cells upon environmental changes, *Lab Chip*, 7, 71-76.

Hersen, P., *et al.* (2008) Signal processing by the HOG MAP kinase pathway, *Proc Natl Acad Sci U S A*, 105, 7165-7170.

Klipp, E., *et al.* (2005) Integrative model of the response of yeast to osmotic shock, *Nat Biotechnol*, 23, 975-982.

Mettetal, J.T., *et al.* (2008) The frequency dependence of osmo-adaptation in Saccharomyces cerevisiae, *Science*, 319, 482-484.

Raue, A., *et al.* (2009) Structural and practical identifiability analysis of partially observed dynamical models by exploiting the profile likelihood, *Bioinformatics*, 25, 1923-1929.

Schaber , J. (2012) Easy parameter identifiability analysis with COPASI, *BioSystems*, accepted.

Schaber, J., *et al.* (2010) Biophysical properties of Saccharomyces cerevisiae and their relationship with HOG pathway activation, *Eur Biophys J*, 39, 1547-1556.

Schaber, J. and Klipp, E. (2008) Short-term volume and turgor regulation in yeast, *Essays Biochem*, 45, 147-159.

Schaber, J. and Klipp, E. (2011) Model-based inference of biochemical parameters and dynamic properties of microbial signal transduction networks, *Curr Opin Biotechnol*, 22, 109-116.

Seber, G.A.F. and Wild, C.J. (2003) *Nonlinear Regression*. Wiley-Interscience.

13 Supplementary Data

The source data for Supplementary Figure S2 is provided in a separate file.

The COPASI and SBML model together with data used by the COPASI model for fitting and ranking are also provided in a separate file.